

Competing phases and suppression of superconductivity in hole-doped Hubbard model on honeycomb lattice

Hao Zhang(张浩), Shaojun Dong(董少钧), and Lixin He(何力新)

Citation: Chin. Phys. B, 2025, 34 (**7**): 077102. DOI: 10.1088/1674-1056/adcb20
http://cpb.iphy.ac.cn; http://iopscience.iop.org/cpb

What follows is a list of articles you may be interested in

Quantitative determination of the critical points of Mott metal—insulator transition in strongly correlated systems

Yuekun Niu(牛月坤), Yu Ni(倪煜), Jianli Wang(王建利), Leiming Chen(陈雷鸣), Ye Xing(邢晔), Yun Song(宋筠), and Shiping Feng(冯世平)
Chin. Phys. B, 2024, 33 (**1**): 017102. DOI: 10.1088/1674-1056/ad0719

Relevance of 3d multiplet structure in nickelate and cuprate superconductors

Mi Jiang(蒋密)
Chin. Phys. B, 2021, 30 (**10**): 107103. DOI: 10.1088/1674-1056/abf646

Benchmarking the simplest slave-particle theory with Hubbard dimer

Wei-Wei Yang(杨薇薇), Hong-Gang Luo(罗洪刚), Yin Zhong(钟寅)
Chin. Phys. B, 2019, 28 (**10**): 107103. DOI: 10.1088/1674-1056/ab3dfe

Hubbard model on an anisotropic checkerboard lattice at finite temperatures: Magnetic and metal-insulator transitions

Hai-Di Liu(刘海迪)
Chin. Phys. B, 2019, 28 (**10**): 107102. DOI: 10.1088/1674-1056/ab4279

Mott transition in ruby lattice Hubbard model

An Bao(保安)
Chin. Phys. B, 2019, 28 (**5**): 057101. DOI: 10.1088/1674-1056/28/5/057101

Competing phases and suppression of superconductivity in hole-doped Hubbard model on honeycomb lattice

Hao Zhang(张浩)[1], Shaojun Dong(董少钧)[2], and Lixin He(何力新)[1,2,3,†]

[1] *CAS Key Laboratory of Quantum Information, University of Science and Technology of China, Hefei* 230026, *China*
[2] *Institute of Artificial Intelligence, Hefei Comprehensive National Science Center, Hefei* 230088, *China*
[3] *Hefei National Laboratory, University of Science and Technology of China, Hefei* 230088, *China*

(Received 24 February 2025; revised manuscript received 9 April 2025; accepted manuscript online 10 April 2025)

We investigate the hole-doped Hubbard model on a honeycomb lattice using a fermionic projected entangled pair states (fPEPS) method. Our study reveals the presence of quasi-long-range order of Cooper pairs, characterized by power-law decay of correlation functions with exponents $K > 1$. We further analyze the competing phases of superconductivity, specifically the antiferromagnetic (AFM) order and the charge density wave (CDW) order. Our results show that there are domain wall structures when the hole doping δ is small and the Coulomb parameter U is large. However, these structures disappear as we increase the hole doping δ or decrease U. Furthermore, for small hole doping, the system exhibits AFM order, which diminishes for $\delta > 0.05$. Conversely, as the doping level increases, the CDW order gradually decreases. Notably, a considerable CDW order persists even at higher doping levels. These findings suggest a progressive suppression of the AFM order and a growing prominence of the CDW order with increasing δ.

Keywords: Hubbard model, honeycomb lattice, superconductivity, fermionic projected entangled pair states

PACS: 71.10.Fd, 74.25.Dw, 73.22.Pr, 02.70.–c

DOI: 10.1088/1674-1056/adcb20 **CSTR:** 32038.14.CPB.adcb20

1. Introduction

The understanding of the high-T_c superconductivity[1,2] stands as one of the foremost challenges in contemporary condensed matter physics. It is believed that the high-T_c superconductivity (SC) can be understood through the study of doped Mott insulators,[3] where the Hubbard model[4] serves as the fundamental framework for describing these insulators. Nevertheless, studies spanning several decades have demonstrated that the raw Hubbard model on a square lattice does not yield a stable superconducting state.[5–7] This has led to increased interest in using the (extended-)Hubbard model to study electron–electron correlations on honeycomb lattices.[8–26] The honeycomb lattice is distinguished from the square lattice by its hexagonal structure, which confers unique electronic properties. The band structure of the honeycomb lattice features Dirac cones at the Fermi level, and with $1/8$ electron and hole doping, it exhibits a logarithmic Van Hove singularity along with significant nesting of the Fermi surface. These characteristics may promote a long-range SC phase on the honeycomb lattice, as discussed in prior studies.[8,19]

While a phase transition from a semimetal to antiferromagnetism has been observed at approximately $U_c = 3.8$ along the half-filling line,[27,28] the impact of doping on the antiferromagnetic state in the Hubbard model on the honeycomb lattice is still not thoroughly understood. Numerous studies have investigated superconductivity on the honeycomb lattice, yielding controversial results. A weak-coupling renormalization group (WCRG) analysis[25] predicts that a stable superconducting phase emerges in the Hubbard model on the honeycomb lattice. A variational quantum Monte Carlo (QMC) study of the Hubbard model on the honeycomb lattice has proposed the existence of superconductivity with chiral $\mathrm{d}+\mathrm{i}\mathrm{d}$ pair symmetry in doped graphene.[8] Additionally, a QMC simulation has predicted the emergence of chiral $\mathrm{d}+\mathrm{i}\mathrm{d}$-wave superconductivity in the strong interaction regime.[9] Furthermore, a Grassmann tensor product states (GTPS) investigation has also demonstrated the presence of a chiral superconductive state in the large U limit, within the context of the t–J model.[29] However, recent findings from a density matrix renormalization group (DMRG) simulation have contradicted these results, indicating a lack of quasi-long-range order in Cooper pair correlation within the doped Hubbard model on the honeycomb lattice.[30] A finite-temperature determinant quantum Monte Carlo (DQMC) result[23] suggests that the hopping terms for second- and third-nearest neighbors play a crucial role in the formation of superconductivity.

However, these numerical methods each have their respective limitations. VMC methods depend on a preset ansatz based on prior knowledge of the ground state, which may lead to biased results. The DMRG method is effective for one-dimensional or quasi-one-dimensional systems but may not

†Corresponding author. E-mail: helx@ustc.edu.cn

© 2025 Chinese Physical Society and IOP Publishing Ltd. All rights, including for text and data mining, AI training, and similar technologies, are reserved.

adequately capture the characteristics of two-dimensional systems. Furthermore, the GTPS wave functions in Ref. [29] are optimized using the simple update scheme,[31] which involves approximations to the environment and may compromise the accuracy of the results.

In this work, we investigate the hole-doped Hubbard model on the honeycomb lattice across a broad parameter range, employing the state-of-the-art fermionic projected entangled pair states (fPEPS) method.[29,32–36] The fPEPS wave functions are optimized using the gradient descent method combined with direct sampling techniques,[37] ensuring controlled accuracy.[34,38–41] This approach, on one hand, avoids errors that arise from neglecting environmental influences during simple update optimization.[31] On the other hand, it significantly reduces the scaling with respect to the bond dimension D compared to the direct contraction method. As a result, it enables the utilization of a substantially larger bond dimension, leading to highly precise and converged results, even for large systems. We observe the presence of quasi-long-range SC order, characterized by a power-law decay of the correlation of Cooper pairs with respect to their separation with decay exponent $K > 1$. We also investigate the competing phases in the system, including the charge density wave (CDW) order and AFM order. We find that at low doping concentrations, the ground state exhibits AFM order. However, this order diminishes progressively with increasing levels of doping, and ultimately diminishes for $\delta > 0.05$. In contrast, the ground states consistently exhibit a persistent CDW order even at a relatively large doping level.

2. Method

The Hamiltonian of the Hubbard model is given by

$$H = -t \sum_{\langle i,j\rangle,\sigma} (c^{\dagger}_{i,\sigma} c_{j,\sigma} + \text{h.c.}) + U \sum_{i} n_{i\uparrow} n_{i\downarrow}, \tag{1}$$

where t and U are the hopping parameter between neighboring sites and the on-site Coulomb interaction, respectively. Here, $c_{i,\sigma}$ represents the annihilation operator for the electron with spin σ at site i, and $n_{i\sigma} = c^{\dagger}_{i\sigma} c_{i\sigma}$. Without loss of generality, $t = 1$ is used in this paper.

The many-particle wave functions of the Hamiltonian are represented by the fPEPS. Details of the fPEPS wave functions can be found in Ref. [34]. In order to simplify the implementation, we map the honeycomb lattice to a square lattice as illustrated in Fig. 1. For each site on the square lattice, we define a tensor composed of two sites on the honeycomb lattice, except for the two corner tensors. Therefore, each tensor has $4^2 = 16$ physical dimensions.

We begin by optimizing the fPEPS wave functions through the application of the simple update scheme.[31] The resulting fPEPSs then serve as the initial states for further optimization via the gradient descent method.[34,38,42] Throughout the optimization process, the total particle number remains conserved, ensuring compliance with the doping concentration. This is achieved by enforcing the $U(1)$ symmetry of the fPEPS.[43] During the simple update, we truncate the virtual dimensions at each step by sorting the singular values and retaining the largest singular ones, which determine the quantum numbers. These quantum numbers of the virtual space, determined by the simple update procedure, are then used in the gradient descent optimization. To calculate the energy and gradients, we employ the direct sampling technique introduced in Ref. [37]. This approach is highly efficient because it avoids correlations between sampled configurations. We start from bond dimension $D = 4$, and gradually increase the bond dimension to $D = 16$, which converges the energy to about 10^{-3} (see Appendix A). The truncation dimension is set to $D_c = 2D$ and the sampling number $N = 10^4$ is used during the optimization of fPEPSs.

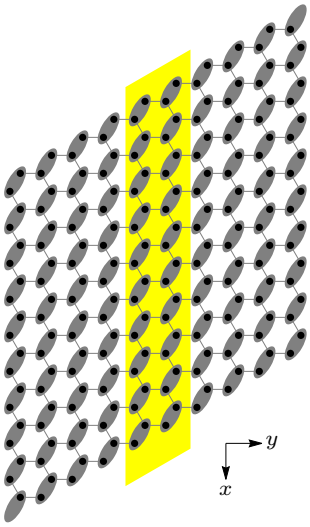


Fig. 1. Mapping of the honeycomb lattice to a square lattice for the fPEPS method. Each gray ellipse corresponds to a singular tensor within the fPEPS framework, encompassing two honeycomb lattice sites, with the exception of the bottom-left and top-right corners, which comprise only a single site. The yellow region indicates the selected region used to calculate the Cooper pair correlation functions.

Once we acquire the ground state wave functions, the physical quantities and correlation functions are computed using direct sampling techniques.[37] The sampling number is set at 10^5 to ensure high accuracy. Additionally, a truncation dimension of $D_c = 6D$ is employed to minimize truncation errors.

3. Results and discussion

3.1. Superconductivity

We first examine the potential for superconductivity in the hole-doped Hubbard model on the honeycomb lattice. On the

honeycomb lattice, singlet and triplet Cooper pair functions are defined as follows:

$$\Delta_a^{\mathrm{s}}(i) = (c_{i\uparrow}c_{j\downarrow} - c_{i\downarrow}c_{j\uparrow})/\sqrt{2}, \tag{2}$$

$$\Delta_a^{\mathrm{t}}(i) = (c_{i\uparrow}c_{j\downarrow} + c_{i\downarrow}c_{j\uparrow})/\sqrt{2}, \tag{3}$$

where $j = i + a$, a is one of the three bond directions around site i. The Cooper pairs can be further classified by their symmetry, which are linear combinations of the $\Delta_a^{\mathrm{s}}(i)$ and $\Delta_a^{\mathrm{t}}(i)$. Note that we do not impose any symmetry constraints on the wave function in our fPEPS ansatz when obtaining the ground state. After optimizing this ground-state wave function, we then analyze the correlation functions of different symmetry components within the same wave function. More details are given in Appendix B.

There are some evidences to support the existence of superconductivity in Hubbard models on the honeycomb lattice from previous studies.[8,9,11] For example, vQMC studies have demonstrated a constant correlation of singlet Cooper pairs in the Hubbard model at $U = 2.4$ and $\delta = 0.2$.[8] Additionally, a variational method based on GTPS has shown non-zero Cooper pairs over a wide region in the large U limit (i.e., the t–J model), indicating the potential existence of superconductivity in the system.[29] Nevertheless, the correlation functions of the Cooper pairs were not computed in their study. However, very recent DMRG and vQMC calculations suggested that superconductivity does not exist in the Hubbard model on the honeycomb lattice.[30] The study found a finite correlation length for the Cooper pairs. To investigate the possibility of superconductivity in these states, we computed the pair correlation functions within a region spanning two columns, as illustrated in Fig. 1.

The pair correlation functions are defined as follows:

$$C(\Delta r) = \frac{1}{N} \sum_{|r_1 - r_2| = \Delta r} |\langle \Delta(r_1)^\dagger \Delta(r_2) \rangle|, \tag{4}$$

where r_1 and r_2 are sites that satisfy $|r_1 - r_2| = \Delta r$ along the path depicted in Fig. 1. These correlation functions are averaged over the N pairs of correlation functions with the same Δr. For $\delta = 0$, the ground state is an antiferromagnetic (AFM) insulator, and the correlation functions should decay exponentially, which is confirmed by our numerical calculations, as shown in Fig. C1 in Appendix C.

Figure 2 depicts the correlation functions at different doping levels for $U = 8$. Specifically, figure 2(a) displays the correlation functions for $\delta = 0.05$. Both the singlet and triplet correlation functions exhibit algebraic decay, i.e., $C(\Delta r) \propto \Delta r^{-K}$. However, the fitted decay parameters, $K^{\mathrm{s}} \sim K^{\mathrm{t}} = 3.8$, are very large, indicating that the correlation functions rapidly approach zero. Here, K^{s} represents the decay parameter for the singlet, and K^{t} for the triplet. These results suggest that superconductivity is suppressed in this regime. It is intriguing to observe that the singlet and triplet pairing correlations exhibit similar power-law decay, which contrasts with the behavior seen in square lattices. This result may be attributed to the higher symmetry of the hexagonal lattice compared to that of the square lattice. The enhanced symmetry of the hexagonal lattice may reduce the differentiation between the singlet and triplet pairing channels, allowing both types of pairing to be similarly stabilized within the system. This observation is particularly interesting, as it suggests that the lattice symmetry plays a significant role in the pairing behavior. We believe this result warrants further investigation.

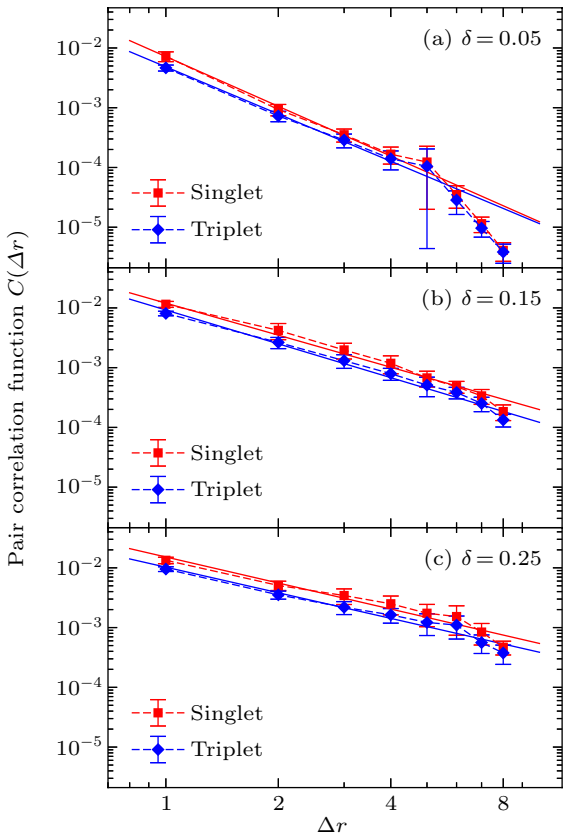


Fig. 2. The Cooper pair correlation functions $C(\Delta r)$ for both singlet and triplet states evaluated at $U = 8$ for different levels of hole doping δ on a 198-site honeycomb lattice. Both the correlation functions and Δr are on a logarithmic scale. The solid lines are fitted using the power-law decay function $C(\Delta r) \propto \Delta r^{-K}$.

Figures 2(b) and 2(c) show the correlation functions for $\delta = 0.15$ and 0.25, respectively. Similar to the $\delta = 0.05$ case, these correlation functions also exhibit power-law decay. The fitted decay parameters K decrease as the doping level increases. For $\delta = 0.15$, $K \sim 1.5$, whereas $K \sim 1.2$ for $\delta = 0.25$. Similar power-law decay was also found in the t–J model on the triangular lattice.[44]

We conducted simulations of the Hubbard model, spanning a range of values for the parameter U from 4 to 12, while exploring different levels of doping. Since previous works

suggest that when $U < U_c \approx 3.8$, the honeycomb lattice becomes a semimetal over a wide doping range,[27,28] we do not study the cases for $U < 4$. Our findings consistently reveal power-law decay behavior in the correlation functions within these specific parameter regimes. The decay exponents for both singlet (K^s) and triplet (K^t) correlations are summarized in Fig. 3. There are several notable trends from the figure. As the doping level increases, the values of the exponents K^s and K^t tend to decrease. For $U = 4$ and doping level δ exceeding 0.05, the parameters K are consistently found to be less than 2. In the case of $\delta = 0.2$, both K^s and K^t approximate a value of 1. Also, for $U = 8$ and δ values greater than 0.1, the exponents K continue to remain below 2, suggesting that SC susceptibility diverges as the temperature approaches 0.[45] It was suggested that long-range SC order may develop near the Van Hove doping.[8,19] However, the results in Fig. 3 near $1/8$ doping do not show significant behaviors.

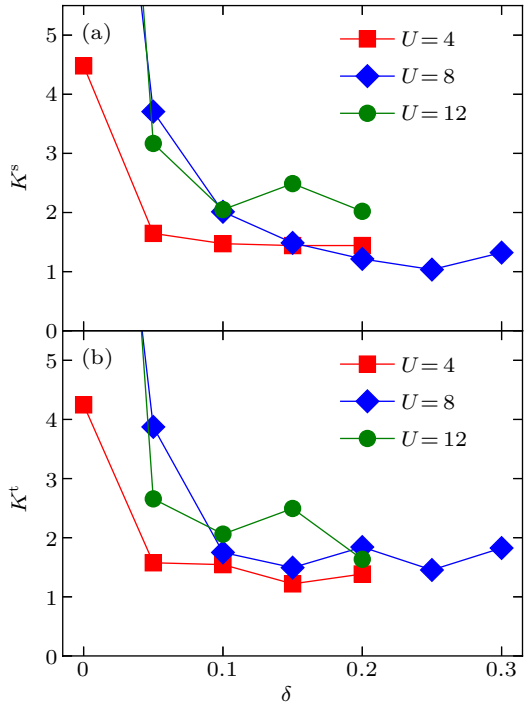


Fig. 3. The power-law decay exponent (a) K^s of the singlet pair correlation functions and (b) K^t of the triplet pair correlation functions as a function of hole doping δ, for different interaction strengths U, on a 198-site honeycomb lattice.

At $\delta = 0.25$, K_s approaches a value of 1. However, when U reaches 12, and $\delta = 0.15$, the values of K exceed those observed at other hole concentrations. This may be attributed to the presence of a competing order that suppresses the SC phase. Remarkably, it is worth noting that these results remain consistent even when employing the symmetrized Cooper pair wave functions, as defined in Appendix B, for calculating the pair correlation functions.

In a previous investigation, Qin employed DMRG calculations to analyze the Hubbard model on a honeycomb lattice, suggesting that the superconducting orders undergo exponential decay.[30] Notably, these calculations were conducted on a long narrow quasi-1D lattice. Our results demonstrate a power-law decay in pair correlations for distances up to $\Delta r < 8$, wherein the pair correlation values approximate 10^{-5}–10^{-4} at $\Delta r = 8$. Within this distance range, our findings align with those reported in Ref. [30]. However, the results in Ref. [30] show a much faster decay for $\Delta r > 8$, which can be fitted with an exponential function. This divergence may stem from the narrow quasi-1D lattice used in Ref. [30]. In Ref. [45], a power-law decay of Cooper pair correlations was also observed. However, it is worth noting that the decay exponents reported in that paper are smaller compared to the ones obtained in our study.

3.2. Anti-ferromagnetic order and charge-density wave order

We now explore the competing phases to the SC order. The two most observed competing phases are the AFM order and the charge density wave (CDW) order. Figure 4 shows the hole density $n_h = 1 - n_\uparrow - n_\downarrow$ and spin density $S_z = \frac{1}{2}(n_\uparrow - n_\downarrow)$ for a system with $U = 12$ and $\delta = 0.05$ on a 198-site lattice. In this figure, the size of the circle corresponds to the hole density, while the color indicates the direction and magnitude of the spin density. The system exhibits a weak antiferromagnetism with a domain wall structure. The spatial variation in hole density suggests the possible presence of a CDW order. Recent DMRG results also reveal a stripe state for both charge and spin within the range $1/16 < \delta < 1/12$ with $U = 8$ in a long and narrow honeycomb lattice, up to 4×32 lattice sites.[30] The stripes in their work are oriented vertically to the long side boundary of the system, which may be due to the lattice size and the cylinder boundary condition. Our results provide additional evidences for the stripe pattern.

The domain wall structure is present for small $\delta = 0.05$ and large values of U. However, as U decreases to $U = 8$, the domain wall structure weakens and is completely absent at $U = 4$. On the other hand, when δ increases to 0.10, the domain wall structure also disappears.

In order to obtain a more quantitative description of the ground state, we calculate the order parameters of CDW and AFM from the structure factors of holes density and spins, which are defined as

$$S_h(\boldsymbol{k}) = \frac{1}{\delta^2 N^2} \sum_{i,j} \langle n_h^i n_h^j \, e^{2\pi i (\boldsymbol{R}_i - \boldsymbol{R}_j)\cdot \boldsymbol{k}} \rangle, \tag{5}$$

$$S_z(\boldsymbol{k}) = \frac{1}{N^2} \sum_{i,j} \langle S_z^i S_z^j \, e^{2\pi i (\boldsymbol{R}_i - \boldsymbol{R}_j)\cdot \boldsymbol{k}} \rangle, \tag{6}$$

where N is the total number of sites in the system. To minimize boundary effects, the sites located on the boundary are

excluded from the summation. The resulting order parameters of CDW and AFM for $U = 12$ and $\delta = 0.05$ are depicted in Figs. 5(a) and 5(b), respectively. The result shows a CDW order with momentum $(4/3\pi, 0)$, as indicated by the peaks in $S_{\rm h}(\boldsymbol{k})$ at the K points. Similar CDW behaviour has been found in the t–J model on the triangular lattice.[44] Similarly, the AFM order parameter also displays peaks around the K points, indicating AFM state. This is distinct from the AFM state on the square lattice, where the spin structure peak is at (π, π).

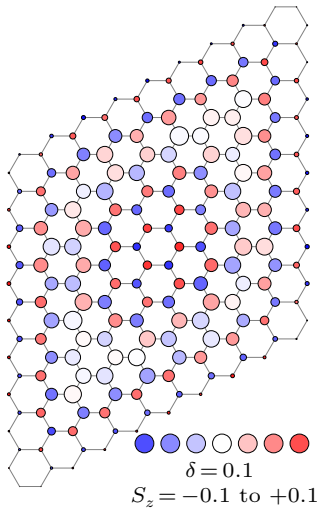


Fig. 4. The hole density $\langle n_{\rm h} \rangle$ and spin $\langle S_z \rangle$ for the ground state of the Hubbard model at $U = 12$ and $\delta = 0.05$, simulated on a 198-site lattice. The color scheme denotes the amplitude of S_z, with red indicating spin-up and blue indicating spin-down. The size of the circle corresponds to the hole density.

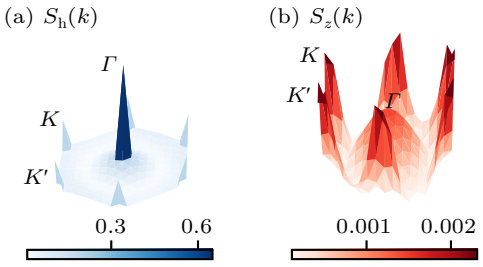


Fig. 5. (a) The CDW order parameter $S_{\rm h}(\boldsymbol{k})$ and (b) AFM order parameter $S_z(\boldsymbol{k})$ at $U = 12$ and $\delta = 0.05$ simulated on a 198-site lattice.

To characterize the overall trend of the system's properties for different values of U and δ, we calculate the order parameter $S_z(K)$ for AFM and $S_{\rm h}(K)$ for CDW. In Figs. 6(a)–6(d), we present the results for U values of 16, 12, 8, and 4, respectively. The AFM order shows similar trends across the different U parameters, i.e., it decreases with increasing hole doping δ. Likewise, the CDW order also exhibits similar trends across the different U parameters. At $\delta = 0$, corresponding to an undoped system, the ground state is expected to be AFM for $U > 3.8$,[28] which is confirmed by our calculations. However, as the doping level increases ($\delta > 0$), the AFM order rapidly diminishes, approaching nearly zero at $\delta = 0.1$. Conversely, at $\delta = 0.05$, we observe a substantial CDW order, indicated by a large value of $S_{\rm h}(K)$. As the doping level increases further, the CDW order gradually decreases. Nevertheless, even at relatively high doping levels such as $\delta = 0.2$, a considerable CDW order persists. These findings suggest a transition from an AFM ground state at $\delta = 0$ to a CDW-dominated state as the doping level increases. The AFM order is progressively suppressed, while the CDW order becomes more prominent. A significant CDW order persists even at higher doping levels.

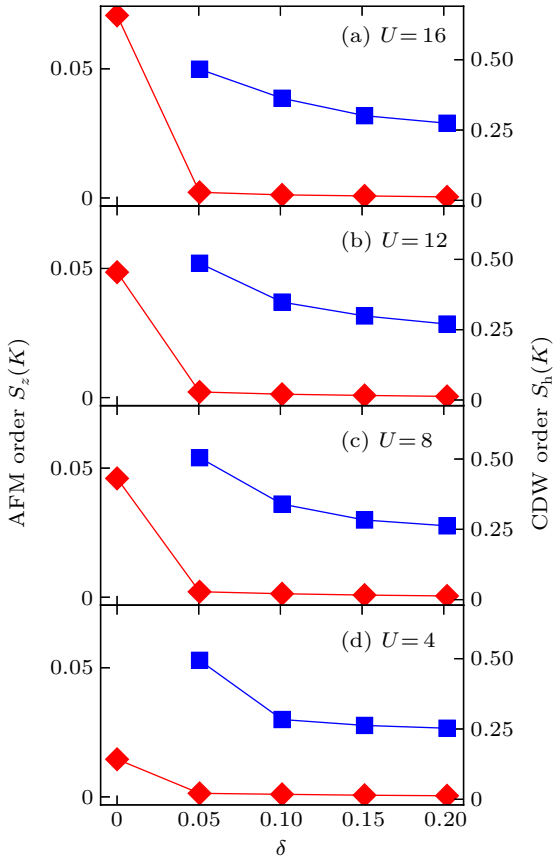


Fig. 6. The order parameters of AFM ($S_z(K)$ shown in red diamonds) and CDW ($S_{\rm h}(K)$ depicted as blue squares) for (a) $U = 4$, (b) $U = 8$, (c) $U = 12$, and (d) $U = 16$, ranging from $\delta = 0.00$ to $\delta = 0.20$, simulated on a 198-site honeycomb lattice.

To investigate the influence of finite size effects, we examine the AFM order and CDW order for different lattice sizes as a function of hole doping δ, specifically for the case where $U = 12$. The corresponding findings are illustrated in Fig. 7. We observe that as the lattice size increases, the results for the AFM and CDW orders converge. Notably, the finite size effects already become small at the 198-site lattice. Therefore, the results obtained for this lattice size can be considered as a reliable approximation for characterizing the ground state properties of the system.

The relationship between SC and CDW is a topic of ongoing research. While it is widely believed that SC and CDW are

competing phases, there are studies suggesting that SC order and CDW can coexist, as exemplified in Refs. [46,47]. Therefore, this remains an active area of research, and the interplay between these phases is still an open question.

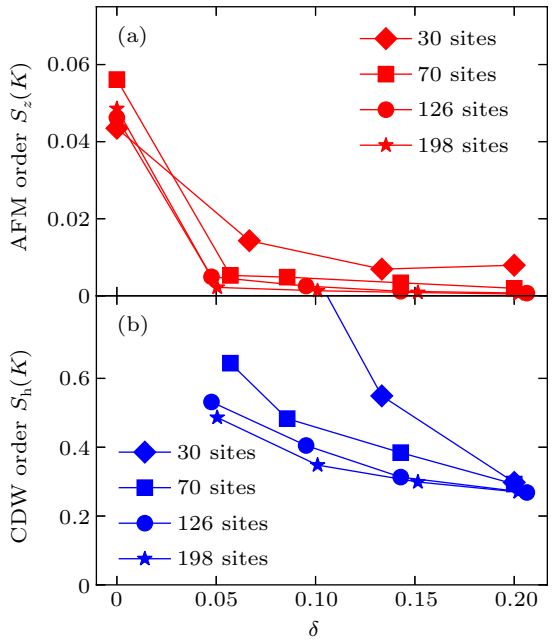


Fig. 7. (a) $S_z(K)$ and (b) $S_h(K)$ as functions of δ at $U = 12$, simulated on lattices of different sizes.

4. Summary

We investigate the ground states of the hole-doped Hubbard model on honeycomb lattices employing the fPEPS method. We explore a wide range of hole doping levels, from $\delta = 0$ to 0.25, and the interaction strengths spanning from $U/t = 4$ to 16. Our results reveal that in a broad parameter space, the Cooper pairs exhibit quasi-long-range order, following a power-law decay, where the decay exponents K are larger than 1, but smaller than 2.

Moreover, our study unveils that at low doping concentrations, the ground state manifests AFM order. However, this order progressively diminishes with increasing levels of doping, ultimately vanishing for $\delta > 0.05$. In contrast, the ground states consistently exhibit a persistent CDW order. These observations suggest a transition from an AFM-dominated ground state at $\delta = 0$ to a state increasingly dominated by CDW as the doping level rises. Furthermore, in the region of large U and small δ, the systems display an evident domain wall structure.

Appendix A: Convergence of energy with bond dimension D

Figure A1 shows the energy of the system as a function of the reciprocal of bond dimension D. The system has a lattice size of 10×10 (198 sites) with $U = 8$ and $\delta = 0.1$. As we can see from the figure, the energy converges to approximate 10^{-3} as D approaches 16.

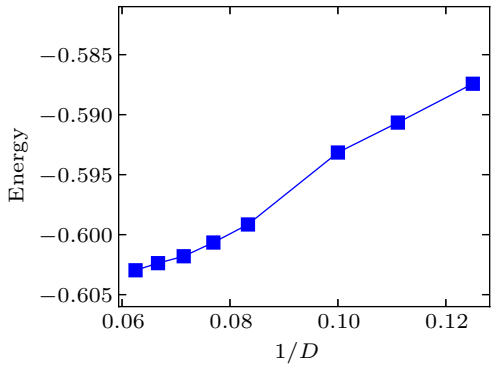


Fig. A1. Convergence of energy as a function of $1/D$ for a 10×10 lattice with $U = 8$ and $\delta = 0.1$.

Appendix B: The Cooper pair pairing symmetries

Systems with superconductivity can be categorized based on their Cooper pair pairing symmetry. On a honeycomb lattice, the possible Cooper pair symmetries are defined in Ref. [48] as combinations of singlet or triplet pairs, expressed as follows:

$$\Delta_{\mathrm{s}}(i) = \Delta_1^{\mathrm{s}}(i) + \Delta_2^{\mathrm{s}}(i) + \Delta_3^{\mathrm{s}}(i), \tag{B1}$$

$$\Delta_{\mathrm{d+id}}(i) = \Delta_1^{\mathrm{s}}(i) + \mathrm{e}^{2\pi\mathrm{i}/3}\Delta_2^{\mathrm{s}}(i) + \mathrm{e}^{4\pi\mathrm{i}/3}\Delta_3^{\mathrm{s}}(i), \tag{B2}$$

$$\Delta_{\mathrm{d-id}}(i) = \Delta_1^{\mathrm{s}}(i) + \mathrm{e}^{-2\pi\mathrm{i}/3}\Delta_2^{\mathrm{s}}(i) + \mathrm{e}^{-4\pi\mathrm{i}/3}\Delta_3^{\mathrm{s}}(i), \tag{B3}$$

$$\Delta_{\mathrm{f}}(i) = \Delta_1^{\mathrm{t}}(i) + \Delta_2^{\mathrm{t}}(i) + \Delta_3^{\mathrm{t}}(i), \tag{B4}$$

$$\Delta_{\mathrm{p+ip}}(i) = \Delta_1^{\mathrm{t}}(i) + \mathrm{e}^{2\pi\mathrm{i}/3}\Delta_2^{\mathrm{t}}(i) + \mathrm{e}^{4\pi\mathrm{i}/3}\Delta_3^{\mathrm{t}}(i), \tag{B5}$$

$$\Delta_{\mathrm{p-ip}}(i) = \Delta_1^{\mathrm{t}}(i) + \mathrm{e}^{-2\pi\mathrm{i}/3}\Delta_2^{\mathrm{t}}(i) + \mathrm{e}^{-4\pi\mathrm{i}/3}\Delta_3^{\mathrm{t}}(i). \tag{B6}$$

Here, Δ_1, Δ_2, and Δ_3 refer to the Cooper pairs associated with the three bonds shown in Fig. B1.

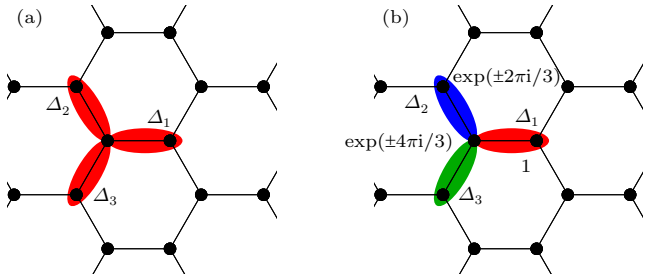


Fig. B1. Illustration of Cooper pair pairing symmetry: (a) for the s and f wave pairing, the three Cooper pairs have unitary phases; (b) for the p and d wave pairing, the three Cooper pairs Δ_1, Δ_2 and Δ_3 have unitary, $\exp(\pm 2/3\pi\mathrm{i})$, and $\exp(\pm 4/3\pi\mathrm{i})$ phases, respectively.

Appendix C: The Cooper pair correlation functions for $\delta = 0$

The ground state of the Hubbard model on a honeycomb lattice with $\delta = 0$ exhibits an AFM state, and consequently, the

Cooper pair correlation functions are expected to decay exponentially. This behavior is supported by the numerical results depicted in Fig. C1 for U values of 4, 8, and 12, respectively.

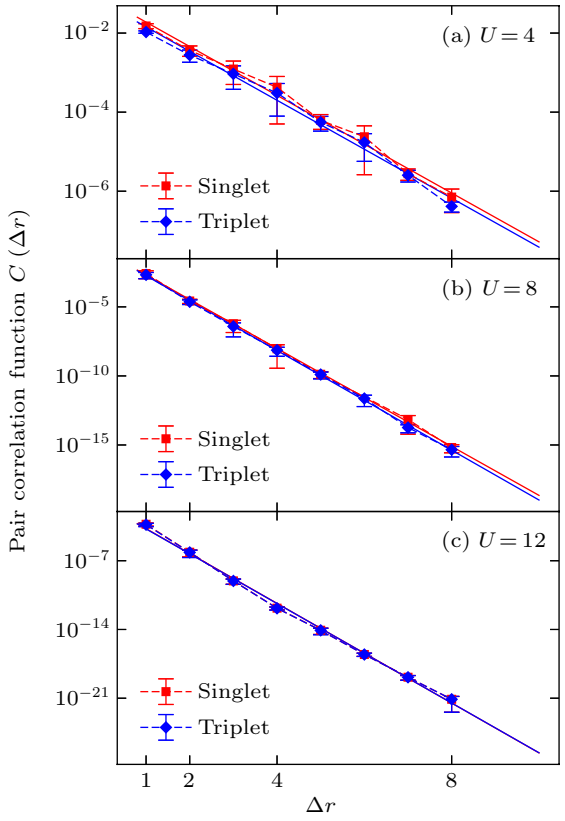


Fig. C1. The Cooper pair correlations decay exponentially for $\delta = 0$ with (a) $U = 4$, (b) $U = 8$, and (c) $U = 12$ on a 198-site honeycomb lattice.

Acknowledgments

We thank Hongchen Jiang for helpful discussion. Project supported by the National Natural Science Foundation of China (Grant Nos. 12134012 and 12104433). The numerical calculations were performed on the USTC HPC facilities.

References

[1] Bednorz J G and Müller K A 1986 *Z. Phys. B: Condens. Matter* **64** 189
[2] Wu M K, Ashburn J R, Torng C J, Hor P H, Meng R L, Gao L, Huang Z J, Wang Y Q and Chu C W 1987 *Phys. Rev. Lett.* **58** 908
[3] Lee P A, Nagaosa N and Wen X G 2006 *Rev. Mod. Phys.* **78** 17
[4] Hubbard J 1963 *Proc. R. Soc. Lond. A* **276** 238
[5] Rozhkov A V and Rakhmanov A L 2011 *J. Phys.: Condens. Matter.* **23** 065601
[6] Kitatani M, Schäfer T, Aoki H and Held K 2019 *Phys. Rev. B* **99** 041115
[7] Qin M, Chung C M, Shi H, Vitali E, Hubig C, Schollwöck U, White S R and Zhang S 2020 *Phys. Rev. X* **10** 031016
[8] Pathak S, Shenoy V B and Baskaran G 2010 *Phys. Rev. B* **81** 085431
[9] Black-Schaffer A M, Wu W and Le Hur K 2014 *Phys. Rev. B* **90** 054521
[10] Wang W S, Xiang Y Y, Wang Q H, Wang F, Yang F and Lee D H 2012 *Phys. Rev. B* **85** 035414
[11] Xu X Y, Wessel S and Meng Z Y 2016 *Phys. Rev. B* **94** 115105
[12] Jiang S, Mesaros A and Ran Y 2014 *Phys. Rev. X* **4** 031040
[13] Gu Z C, Jiang H C and Baskaran G 2020 *Phys. Rev. B* **101** 205147
[14] Kiesel M L, Platt C, Hanke W, Abanin D A and Thomale R 2012 *Phys. Rev. B* **86** 020507
[15] Raghu S, Kivelson S A and Scalapino D J 2010 *Phys. Rev. B* **81** 224505
[16] Honerkamp C 2008 *Phys. Rev. Lett.* **100** 146404
[17] Ying T and Yang S 2020 *Phys. Rev. B* **102** 125125
[18] Wolf S, Schmidt T L and Rachel S 2018 *Phys. Rev. B* **98** 174515
[19] Nandkishore R, Levitov L S and Chubukov A V 2012 *Nat. Phys.* **8** 158
[20] Watanabe T and Ishihara S 2013 *J. Phys. Soc. Jpn.* **82** 034704
[21] Ma T, Yang F, Yao H and Lin H Q 2014 *Phys. Rev. B* **90** 245114
[22] Wu W, Scherer M M, Honerkamp C and Le Hur K 2013 *Phys. Rev. B* **87** 094521
[23] Jia P, Yang S, Li W, Yang J, Ying T, Li X and Sun X 2022 *Phys. Lett. A* **442** 128175
[24] Jin X, Liu Y, Mondaini R and Rigol M 2022 *Phys. Rev. B* **106** 245117
[25] Wolf S, Gardener T, Le Hur K and Rachel S 2022 *Phys. Rev. B* **105** L100505
[26] Zhu X, Han W, Feng S and Guo H 2024 *Physica B* **683** 415902
[27] Lin H F, Liu H D, Tao H S and Liu W M 2015 *Sci. Rep.* **5** 9810
[28] Otsuka Y, Yunoki S and Sorella S 2016 *Phys. Rev. X* **6** 011029
[29] Gu Z C, Jiang H C, Sheng D N, Yao H, Balents L and Wen X G 2013 *Phys. Rev. B* **88** 155112
[30] Qin M 2022 *Phys. Rev. B* **105** 035111
[31] Jiang H C, Weng Z Y and Xiang T 2008 *Phys. Rev. Lett.* **101** 090603
[32] Barthel T, Pineda C and Eisert J 2009 *Phys. Rev. A* **80** 042333
[33] Corboz P, White S R, Vidal G and Troyer M 2011 *Phys. Rev. B* **84** 041108
[34] Dong S J, Wang C, Han Y, Guo G C and He L 2019 *Phys. Rev. B* **99** 195153
[35] Corboz P, Orús R, Bauer B and Vidal G 2010 *Phys. Rev. B* **81** 165104
[36] Kraus C V, Schuch N, Verstraete F and Cirac J I 2010 *Phys. Rev. A* **81** 052338
[37] Vieijra T, Haegeman J, Verstraete F and Vanderstraeten L 2021 *Phys. Rev. B* **104** 235141
[38] Liu W Y, Dong S J, Han Y J, Guo G C and He L 2017 *Phys. Rev. B* **95** 195154
[39] He L, An H, Yang C, Wang F, Chen J, Wang C, Liang W, Dong S, Sun Q, Han W, Liu W, Han Y and Yao W 2018 *IEEE TPDS* **29** 2838
[40] Dong S J, Wang C, Han Y J, Yang C and He L 2020 *npj Quantum Mater.* **5**
[41] Dong S, Zhang H, Wang C, Zhang M, Han Y J and He L 2023 *Chin. Phys. Lett.* **40** 126403
[42] Sandvik A W and Vidal G 2007 *Phys. Rev. Lett.* **99** 220602
[43] Singh S, Pfeifer R N C and Vidal G 2011 *Phys. Rev. B* **83** 115125
[44] Jiang H C 2021 *npj Quantum Mater.* **6** 71
[45] Peng C, Sheng D N and Jiang H C 2025 *Phys. Rev. B* **111** 085108
[46] Morosan E, Zandbergen H W, Dennis B S, Bos J W G, Onose Y, Klimczuk T, Ramirez A P, Ong N P and Cava R J 2006 *Nat. Phys.* **2** 544
[47] Wang Y, Agterberg D F and Chubukov A 2015 *Phys. Rev. Lett.* **114** 197001
[48] Faye J P L, Sahebsara P and Sénéchal D 2015 *Phys. Rev. B* **92** 085121